

Elastic flexural rigidity of steel-concrete composite columns

Mark D. Denavit^{a,*}, Jerome F. Hajjar^b, Tiziano Perea^c, Roberto T. Leon^d

^a Department of Civil and Environmental Engineering, University of Tennessee, Knoxville, TN, United States

^b Department of Civil and Environmental Engineering, Northeastern University, Boston, MA, United States

^c Departamento de Materiales, Universidad Autónoma Metropolitana, Mexico City 02200, Mexico

^d Via Department of Civil and Environmental Engineering, Virginia Tech, Blacksburg, VA, United States

ARTICLE INFO

Keywords:

Steel-concrete composite
Columns
Elastic analysis
Flexural rigidity
Design

ABSTRACT

The use of elastic analysis is prevalent in the design of building structures even under loading conditions where inelasticity would be expected. Accordingly, geometric and material properties used in the elastic analyses must be carefully selected to maintain accuracy. Steel-concrete composite columns experience different forms of inelasticity. Concrete cracking is the source of much of the inelasticity and occurs at relatively low levels of load, but partial yielding of the steel, slip between concrete and steel, and concrete crushing also contribute to losses in stiffness. In this paper, the behavior of composite columns is characterized at the cross section and member levels through comparisons between inelastic and elastic analyses. Then, through a broad parametric study, specific practical design recommendations are developed for the elastic flexural rigidity of composite columns for the determination of lateral drifts under service loads. The recommendations in this paper provide simple and robust values for the stiffness of composite columns to be used for drift computations involving lateral loads.

1. Introduction

Building structures are typically designed with the expectation that they will experience inelasticity during their design life. Different forms of inelastic behavior will occur at different levels of loading. In steel-concrete composite members, concrete cracking may occur under relatively low loads, slip may occur at moderate loads, and steel yielding and concrete crushing may occur relatively high loads. Despite the increasing use of inelastic analysis, which can track this behavior explicitly, elastic analysis remains prevalent in design. Thus, the expected inelasticity must be accounted for implicitly in the elastic analysis. One way of accomplishing this is through appropriate modifications of the geometric and material properties assumed in the analysis.

In elastic analyses with frame elements, the behavior of cross sections is represented by elastic rigidities which define the stiffness of cross sections in various modes of deformation, for example the axial stiffness, EA , the flexural stiffness, EI , the shear stiffness, GA , and the torsional stiffness, GJ . For moment frame systems, the dominant mode of deformation is typically bending, thus EI is of prime importance.

Elastic analyses are used for many different purposes in the design of building structures, and the appropriate elastic geometric and material section properties may differ depending on the purpose of the analysis. For strength design, appropriate elastic section properties typically reflect the level of inelasticity at the “ultimate” limit state.

Alternatively, when computing deflections due to wind loading for story drift checks, appropriate elastic section properties typically reflect the level of inelasticity at a “service loading” level. The elastic section properties used for service loading level design checks are often greater than those for the determination of required strengths. For example, in the *ACI Code*, the moment of inertia is permitted to be increased by a factor of 1.4 for service load analysis [2] and in the *AISC Specification*, the stiffness reductions associated with the direct analysis method are not intended for determining deflections [3].

While a variety of potential uses for elastic flexural rigidity exist, they are not all equally common in practice. All structures are evaluated for strength which typically includes using an elastic flexural rigidity within design equations to determine the compressive strength of columns and within a second-order analysis to determine required strengths. The appropriate effective flexural rigidity for these uses was the subject of recent research and changes to code provisions [3,8]. The evaluation of serviceability drift limits is equally important, especially for moment frames where drift limitations may control the design. However, less attention has been paid to the appropriate effective flexural rigidity for this use. Another common use of the elastic flexural rigidity is within an Eigenvalue analysis to compute fundamental periods for the determination of seismic loads as was investigated by Perea et al. [20]. An example of a less common use of the elastic flexural rigidity is to define the elastic component of a concentrated plasticity

* Corresponding author.

E-mail addresses: mdenavit@utk.edu (M.D. Denavit), jf.hajjar@northeastern.edu (J.F. Hajjar), tperea@azc.uam.mx (T. Perea), rleon@vt.edu (R.T. Leon).

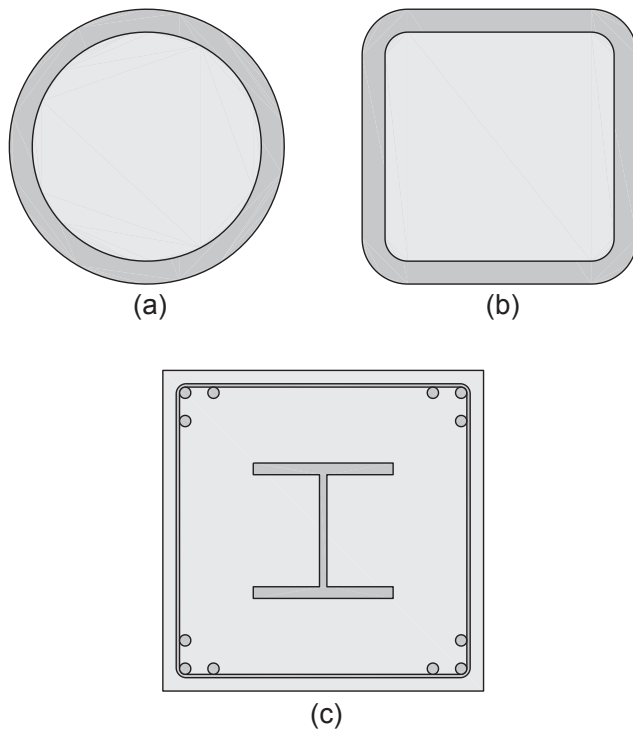


Fig. 1. Composite cross sections.

beam element or other beam element where geometric and material nonlinearity are handled distinctly [22].

In this paper, the stiffness of steel-concrete composite columns is tracked first at the cross-section level then at the member level to provide accurate and practical guidance on the elastic flexural rigidity of such members for the specific purpose of determination of lateral drifts under service loads. Both concrete-filled steel tube (CFT, Fig. 1a and b) and encased or steel-reinforced concrete (SRC, Fig. 1c) columns are investigated. This research focuses on short-term behavior, such as deformations caused by wind loading, and thus the effects of creep and shrinkage are not included.

2. Literature review

Structural steel has a relatively high proportional limit, thus, the use of the gross section properties and modulus of elasticity is widely considered safe and accurate for analysis at service loads. For determination of required strengths per the direct analysis method, a reduction of 0.8 is applied to all stiffness of all members that contribute to the lateral stability of the structure with a further reduction of τ_b on EI (τ_b is a factor that varies between 0 and 1 and depends on the axial compression within the member) [3]. These reductions account for the partial yielding (accentuated by residual stresses) that occurs in members under combined bending and axial load.

Concrete cracks in tension and has a relatively low proportional limit in compression. Several different recommendations and options for the flexural rigidity are given in the ACI Code [2] depending on the use of the value. A relatively low flexural rigidity is used to determine the moment magnification of nonsway frames. Relatively higher flexural rigidities are permitted for use in elastic analyses to determine required strengths or lateral deflections at ultimate loads. Two primary options are given. For the simple option, the flexural rigidity for columns is recommended as 70% of the product of the modulus of elasticity of the concrete and the gross moment of inertia (Eq. (1)) based on the work of MacGregor and Hage [15]. The more complex expression for the flexural rigidity takes into account the effects of load and steel ratio (Eq. (2)). These equations were developed by Khuntia and Ghosh

[11,12] based on parametric computational studies on reinforced concrete cross sections. To determine lateral deflections at service loads, the ACI Code [2] permits the use of Eq. (1) or (2) multiplied by 1.4. Other studies have also focused on the flexural rigidity of reinforced concrete members [16,9,4,13].

$$EI = 0.7E_c I_g \quad (1)$$

$$EI = E_c I \quad (2a)$$

$$I = \left(0.80 + 25 \frac{A_{sr}}{A_g} \right) \left(1 - \frac{M_u}{P_u H} - 0.5 \frac{P_u}{P_{no}} \right) \leq 0.875 I_g \quad (2b)$$

where E_c = modulus of elasticity of concrete, I_g = gross moment of inertia of the cross section, A_{sr} = area of steel reinforcing, A_g = gross area of the cross section, M_u = required bending moment, P_u = required axial compression, H = section depth, and P_{no} = cross-sectional axial capacity.

A variety of approaches and relations have been proposed to evaluate the elastic rigidity of composite members. The different recommendations are not necessarily comparable since they were often developed with different objectives and for different purposes (e.g., determination of axial strength, assessment of deformations, and use in nonlinear finite element formulations).

The effective flexural rigidity, EI_{eff} , given in the AISC Specification [3] is intended for use within a column curve approach to compute the axial compressive strength of composite columns. Different expressions are provided for this rigidity for SRC (Eq. (3)) and CFT (Eq. (4)) members. The effective flexural rigidity is also used, with reductions, for determining required strengths within the direct analysis method (EI_{DA} , Eq. (5)). These expressions are based on computation analyses of small frames as well as an evaluation of column and beam-column experimental results [8]. The expressions are new to the 2016 AISC Specification; previous expressions were similar in form and based solely on evaluations of experimental results [14].

$$EI_{eff} = E_s I_s + E_s I_{sr} + C_1 E_c I_c \quad (\text{SRC}) \quad (3a)$$

$$C_1 = 0.25 + 3 \left(\frac{A_s + A_{sr}}{A_g} \right) \leq 0.7 \quad (3b)$$

$$EI_{eff} = E_s I_s + E_s I_{sr} + C_3 E_c I_c \quad (\text{CFT}) \quad (4a)$$

$$C_3 = 0.45 + 3 \left(\frac{A_s + A_{sr}}{A_g} \right) \leq 0.9 \quad (4b)$$

$$EI_{DA} = 0.64 EI_{eff} \quad (5)$$

where E_s = modulus of elasticity of steel, I_s = moment of inertia of the steel shape, I_{sr} = moment of inertia of the reinforcing, I_c = moment of inertia of the concrete, and A_s = area of the steel shape.

In the ACI Code [2], composite columns are treated much the same as reinforced concrete columns. A slightly different formula is recommended for the determination of the moment magnification for nonsway frames, but, otherwise no special formulas are given.

In Eurocode 4 [5], two equations for the effective flexural rigidity are provided. The first, $(EI)_{eff}$ (Eq. (6)), is for the determination of the member slenderness to be used within a column curve to determine axial strength. The second, $(EI)_{eff,II}$ (Eq. (7)), is to be used within an elastic analysis to determine required strengths. For both equations, the effective rigidity is taken as the sum of the individual components with factors reducing the concrete contribution. For $(EI)_{eff,II}$, an additional reduction factor is applied to the summation.

$$(EI)_{eff} = E_s I_s + E_s I_{sr} + 0.6 E_c I_c \quad (6)$$

$$(EI)_{eff,II} = 0.9(E_s I_s + E_s I_{sr} + 0.5 E_c I_c) \quad (7)$$

Other recommendations can be found in the literature. Schiller et al. [22] summarized published elastic rigidity recommendations for

rectangular concrete-filled steel tubes (RCFT) with a focus on use in nonlinear beam-column element formulations. Axial, flexural, shear, and torsional rigidity were investigated separately. It was determined that for axial and flexural elastic rigidities, using the initial stiffness with the gross section properties is appropriate for defining the elastic component of a concentrated plasticity element. However, an alternative flexural rigidity was recommended for more general use within elastic analysis in which only a portion of the flexural rigidity from the concrete is included. Roeder et al. [21] investigated the flexural rigidity of circular concrete-filled steel tubes (CCFT) through comparisons to available experimental results and proposed a new expression for EI where the concrete contribution depends on the axial load and the steel ratio. Tikka and Mirza [23,24] developed expressions for the flexural rigidity of SRC members through parametric computational studies on composite beam-columns.

3. Behavior of cross sections

Among the simplest nonlinear models for composite cross sections is to assume that plane sections remain plane, the steel behaves elastically, and the concrete behaves elastically in compression but is cracked and can sustain zero stress in tension. These assumptions correspond to a state of moderately low loading after the concrete has cracked, but prior to any significant concrete crushing or steel yielding, and are often used in reinforced concrete design to determine the stiffness of beams [18]. Utilizing these assumptions, the cracked elastic stiffness will depend on the location of the neutral axis and can be expressed in the form of Eq. (8), where the concrete contribution, $C_{cracked}$, for a given cross section depends only on the load eccentricity, e .

$$EI_{cracked} = E_s I_s + E_s I_{sr} + C_{cracked}(e) E_c I_c \tag{8}$$

$$C_{cracked}(e) = \frac{EI_{cracked} - E_s I_s - E_s I_{sr}}{E_c I_c} \tag{9}$$

For a given cross section shape, the concrete contribution can be computed as a function of non-dimensional properties. The concrete contribution factor as a function of the load eccentricity for CCFT sections for a variety of properties is shown in Fig. 2. The results in Fig. 2 were computed by stepping through a series of assumed locations of the neutral axis. For each, $C_{cracked}$ was determined as the ratio of the

moment of inertia of the concrete in compression (i.e., on one side of the neutral axis) to gross moment of inertia of the concrete and the load eccentricity was determined as the ratio of bending moment to axial load, which were both determined per unit curvature based on the neutral axis location. A negative curvature indicates that the section was under net tension. In this case, the concrete contribution is defined only by the load eccentricity normalized with respect to a ratio of the cross section compressive and flexural strengths (P_{no} and M_{no} respectively), the material stiffness ratio E_s/E_c , and the steel ratio A_s/A_g . The cross section strengths are determined in accordance with the AISC Specification [3] noting that, in this study, local buckling is neglected and CFT sections with internal reinforcement are excluded. The cross section axial strength, P_{no} , is given by Eqs. (10) and (11), where C_2 equals 0.85 for rectangular sections and 0.95 for round sections. The cross section moment strength, M_{no} , is determined by the plastic stress distribution method defined within the AISC Specification [3].

$$P_{no} = F_y A_s + F_{ysr} A_{sr} + 0.85 f'_c A_c \tag{10} \text{ (SRC)}$$

$$P_{no} = F_y A_s + C_2 f'_c A_c \tag{11} \text{ (CFT)}$$

where F_y = steel yield stress, F_{ysr} = reinforcing yield stress, and f'_c = concrete compressive strength.

The results of Fig. 2 confirm the bounds of the concrete contribution as 0 when all the concrete is in tension and 1 when all the concrete is in compression. A concrete contribution of around 0.5 indicates that the neutral axis is near the centroid of the cross section, which occurs for a range from about pure bending ($e = \infty$ or $M_{no}/(e P_{no}) = 0$) to $M_{no}/(e P_{no}) = 0.25$. For a better sense of these normalized values, results from the case of a CCFT section with $A_s/A_g = 0.12$ and $E_s/E_c = 7$ are plotted in Fig. 3 on an interaction diagram constructed using the plastic stress distribution method. For the construction of the interaction diagram, the steel yield stress was taken as $F_y = 345$ MPa and the concrete compressive strength was taken as $f'_c = 36.4$ MPa, which corresponds to the selected modular ratio. These results are applicable for any size of CCFT section with the given steel ratio. As noted above, the value of $C_{cracked}$ is near 0.5 for the case of pure bending and increases relatively slowly traversing up the interaction diagram around the balance point. After $M_{no}/(e P_{no}) = 0.5$, $C_{cracked}$ increases rapidly up to the maximum value of 1. A similar pattern can be seen traversing the interaction diagram in tension.

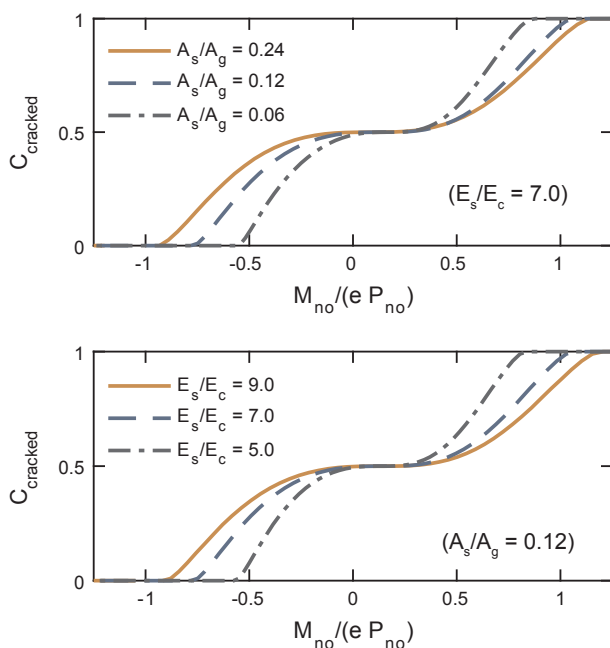


Fig. 2. Cracked elastic concrete contribution factor for CCFT.

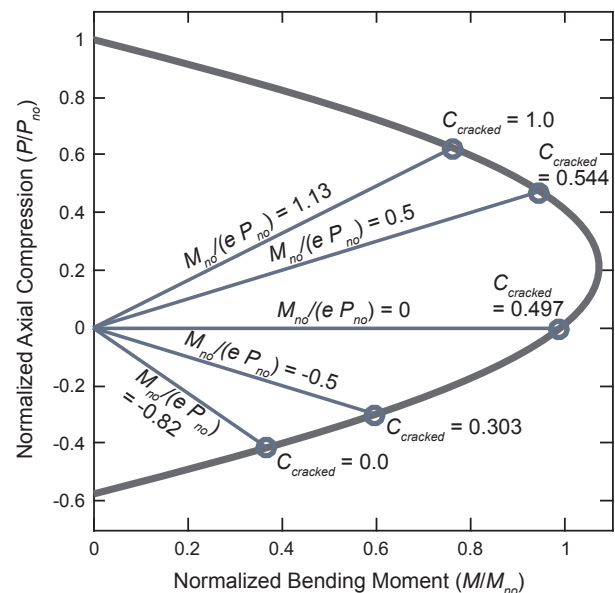


Fig. 3. Example interaction diagram with cracked elastic results.

3.1. Evaluation by inelastic analysis

While analyses that use the “cracked elastic” assumptions described in the previous section can identify aspects of the behavior of composite columns, a more complete picture can be obtained using more accurate and complex constitutive relations for the steel and concrete within fiber analyses. For this type of analysis, the cross section is divided into many small areas, termed fibers, each with an assigned uniaxial constitutive relation. Under a given section deformation (e.g., axial strain at the centroid and curvature) the axial strain at each fiber is calculated assuming that plane sections remain plane (neglecting slip between the steel and concrete); this strain is then used to compute the stress and tangent modulus at each fiber. These values are integrated over the section to obtain section forces (e.g., axial load and bending moment) and stiffness (e.g., EA and EI). The stiffness obtained directly from the integration under any given loading condition is a tangent stiffness and is useful in the analysis; however, the secant stiffness is of more importance to this study since the goal is to recommend stiffness values that, when used in an elastic analysis, result in deformations equivalent to those from an inelastic analysis.

The constitutive relations assigned to the fibers are critical to the accuracy of this method. The following describes the steel and concrete constitutive relations used in this study for SRC and CFT cross sections.

Wide-flange shapes are modeled with elastic-perfectly plastic constitutive relations and the Lehigh residual stress pattern [10]. Reinforcing steel is assumed to have negligible residual stress and is also modeled with an elastic-perfectly plastic constitutive relation. Residual stresses in cold formed steel tubes vary through thickness. To allow a reasonable fiber discretization of the CFT sections, residual stresses are included implicitly in the constitutive relation. A multilinear constitutive relation is used in which the stiffness decreases at 75%, 87.5%, and 100% of the yield stress to approximate the gradual transition into plasticity observed in cold-formed steel (Fig. 4) [1]. In addition, the yield stress in the corner region of the rectangular members is increased to account for the additional work hardening in that region. The increase in yield stress is a function of the ratio of inside bending radius to thickness, which is taken as unity, and the ratio of steel ultimate strength to steel yield strength, F_u/F_y , which is estimated by Eq. (12) [7].

$$F_u/F_y = 1 + 4190F_y [\text{MPa}]^{-1.61} \quad (12)$$

The Popovics model is selected for concrete in compression, with the peak compressive stress taken as f'_c or greater to account for confinement provided by the steel shape and reinforcing [7]. The strain at peak compressive stress, ϵ'_c , is taken as Eq. (13), with increases to account for confinement. Spalling behavior is incorporated into the model

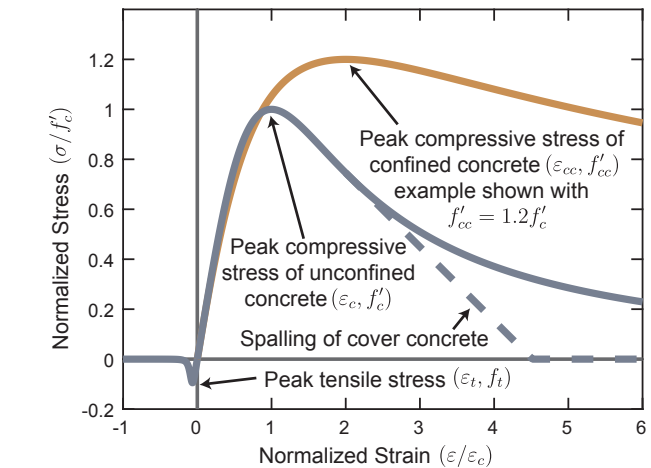


Fig. 5. Concrete constitutive relation.

for the cover concrete of SRC sections by overriding the stress-strain response with linear degradation to zero-stress starting at two times the strain at peak stress (Fig. 5).

$$\epsilon'_c = f'_c [\text{MPa}]^{1/4} / 1150 \quad (13)$$

The modulus of elasticity of concrete used in the analysis is calculated by Eq. (14) taken from the ACI Code [2] for normal weight concrete. Eq. (14) is equivalent to the expression in the AISC Specification [3] when the density is 2372 kg/m^3 . Other expressions for the modulus of elasticity have been proposed as more accurate for high-strength concrete and could have been used in the analysis. However, it is not the intention of this work to develop design recommendations that implicitly include a correction for any potential inaccuracies in the code specified formula for the concrete modulus. It is important to note that Eq. (14) is used as an initial modulus in this work, whereas it is defined as a secant modulus to $0.45f'_c$ within the ACI Code [2].

$$E_c [\text{MPa}] = 4733 \sqrt{f'_c [\text{MPa}]} \quad (14)$$

Concrete in tension is also modeled using Popovics equation noting that the shape of the monotonic tension stress-strain response of concrete has been shown to have a descending branch similar to that of concrete in compression [6]. The peak tensile stress, f'_t , is taken as Eq. (15) and the strain at peak tensile stress, ϵ'_t , is taken as Eq. (16) [26]. Starting at twice the strain at peak stress, Popovics equation is overridden with a linear stress-strain response to zero-stress (Fig. 5). Many of the analyses are performed under non-proportional loading, thus portions of the cross section are subject to a minor strain reversal as they initially are loaded in compression then as the bending moment increases unload and experience tension. The constitutive relations employ cyclic rules [6,7] which handle these reversals with little effect on the results.

$$f'_t [\text{MPa}] = 0.50 \sqrt{f'_c [\text{MPa}]} \quad (15)$$

$$\epsilon'_t = 1.23 f'_t / E_c \quad (16)$$

These constitutive relations have been validated against hundreds of experimental results from composite members under a variety of loading conditions and with a wide range of material and geometric properties [7]. Such comparisons have confirmed the validity of the assumptions made in the development of the model (e.g., neglecting the effect of the hoop stress on the behavior of the steel tube). These constitutive relations have also been used (with the exception of concrete in tension) in previous studies for the development of design recommendations [8]. Since all of the analyses performed in this study are two-dimensional, strips are used for the fiber section. The nominal height of the strips was 1/30th of the section depth (e.g., for a CCFT

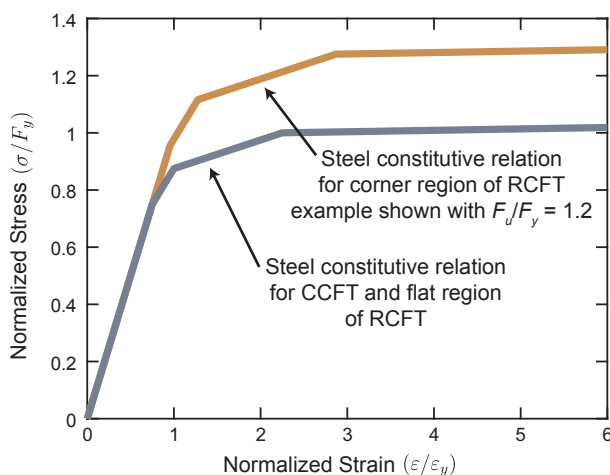


Fig. 4. Steel constitutive relation for CFT.

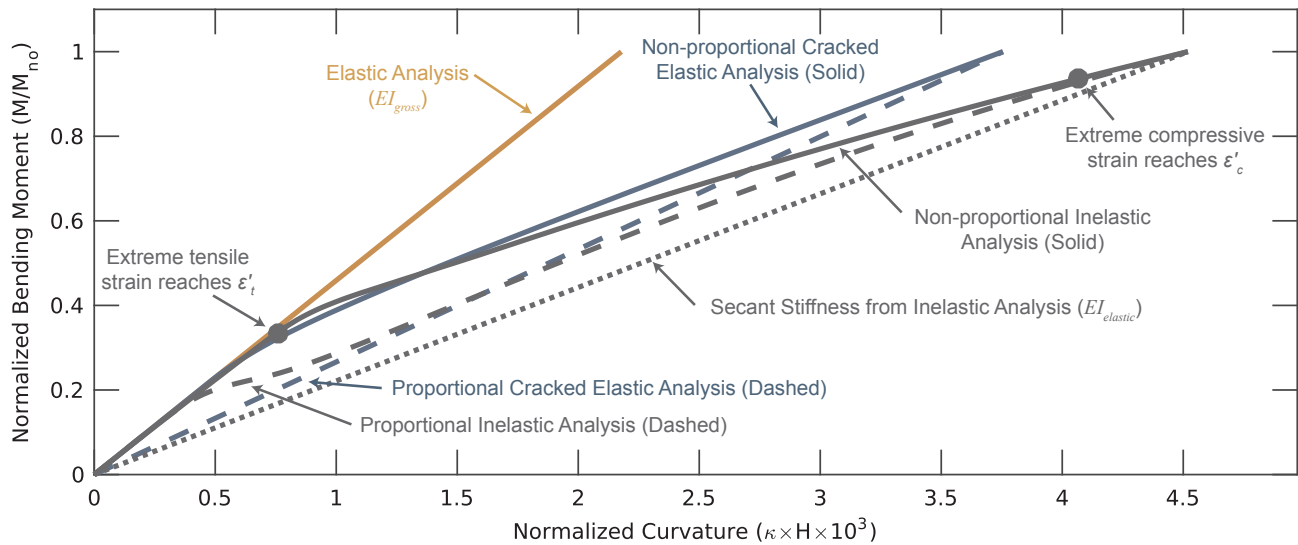


Fig. 6. Cross section moment-curvature analysis results.

section, approximately 30 steel and 30 concrete strips of near equal height were used).

The results of several fiber section analyses on a SRC cross section using different constitutive relations and different loading patterns are shown in Fig. 6. The analyzed cross section has equal outside dimensions of 915 mm and an embedded W360 × 262 steel shape (resulting in a steel ratio of $A_s/A_g = 0.012$). The steel reinforcing is comprised of 12 #32 bars (resulting in a reinforcing ratio of $A_{sr}/A_g = 0.040$) grouped in the corners (such as shown in Fig. 1c) with a clear spacing of 1.5 times the bar diameter. A clear cover of 38 mm is provided between the outside face of the cross section and the lateral reinforcing which is comprised of #10 ties spaced at 305 mm. Material strengths are $f'_c = 28$ MPa, $F_y = 345$ MPa, and $F_{ysr} = 420$ MPa.

Three different constitutive relations were used in the analyses. Results labeled as inelastic analysis use the constitutive relations described in this section. Results labeled as cracked elastic analysis use an elastic constitutive relation for the steel and elastic-no-tension constitutive relation for the concrete as described in the previous section. Results labeled as elastic analysis use elastic constitutive relations for both the steel and concrete. Two different types of loading were used. Under non-proportional loading, an axial compression load of $P = 0.2P_{no} = 6900$ kN was applied then held constant as a bending moment of $M = M_{no} = 4410$ kN m was applied. Note that the moment capacity of the cross section is greater than M_{no} at this level of axial compression. Under proportional loading, the axial compression and bending moment were applied simultaneously with an eccentricity of $e = M_{no}/0.2P_{no} = 639$ mm.

Examining the results of Fig. 6, several observations can be made. First, with the exception of the proportional cracked elastic analysis, the initial stiffness of each of the analyses is nearly identical, confirming that under low loads, the use of gross cross sectional properties (i.e., EI_{gross} , Eq. (17)) is appropriate. Second, the deformation of the inelastic analysis is greater than that of the cracked elastic analysis, indicating that while a portion of the stiffness reduction can be attributed to cracking, other forms of inelasticity must be accounted for when determining appropriate secant stiffness values. In this case, all of the inelasticity comes from the concrete as no yielding occurs in the steel or reinforcing under the applied loads. Two points on the load-deformation curve from the non-proportional inelastic analysis are identified in Fig. 6. The first point is where the extreme tensile strain reaches ϵ'_t (Eq. (16)); this point is associated with cracking and is where significant inelasticity initiates. The second point is where the extreme compressive strain reaches ϵ'_c (Eq. (13)); this point is associated with the initiation of concrete crushing. Third, inelasticity initiates at higher

applied moment under non-proportional loading as compared to proportional loading because the initial compression reduces the tensile strain, thus delaying the opening of cracks.

$$EI_{gross} = E_s I_s + E_s I_{sr} + E_c I_c \quad (17)$$

A key result from Fig. 6, is the secant stiffness from the inelastic analysis. This stiffness is unique to the particular applied loads, but at these applied loads, an elastic analysis that uses this stiffness (termed $EI_{elastic}$ since it is intended to be used within an elastic analysis) would give the same curvature as from the inelastic analysis. In Fig. 7, $EI_{elastic}$ results from many pairs of applied axial load and bending moment are shown. Each dot represents one analysis to determine $EI_{elastic}$; the shade of the dot is representative of the ratio of the resulting value of $EI_{elastic}$ to EI_{gross} , with lighter shades representing lower secant stiffness. The nominal cross section strength interaction diagram [14] is also included, as is the allowable cross section strength interaction diagram which was obtained by factoring each point in the nominal interaction diagram down by a safety factor of 2.0 and left by a safety factor of 1.67 in accordance with the method presented in the commentary to the

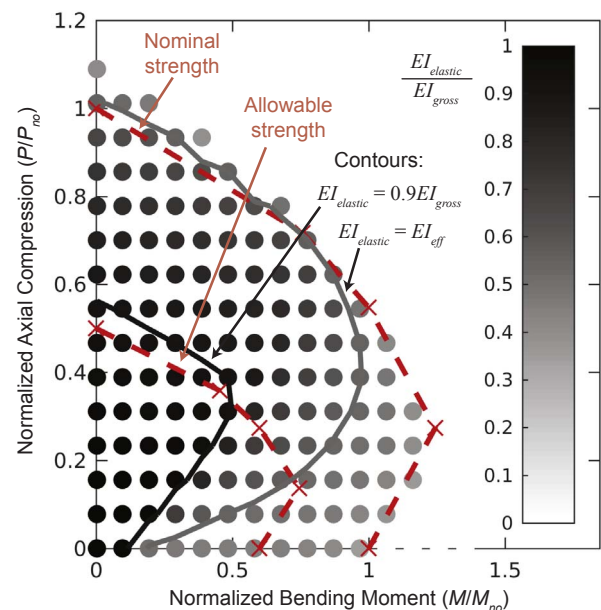


Fig. 7. Cross section secant stiffness results.

AISC Specification [3]. The allowable strength can roughly be considered the upper bound of service level loads. Values of $EI_{elastic}$ were capable of being obtained outside the nominal design interaction diagram because the selected constitutive relations differ somewhat from the assumptions in the plastic stress distribution method.

As expected, the secant stiffness obtained from the inelastic analysis, $EI_{elastic}$, varies significantly with applied loads. Two contours of the results are also shown in Fig. 7, one at $EI_{elastic} = 0.9EI_{gross}$ and one at $EI_{elastic} = EI_{eff}$ (Eq. (3)) ($EI_{eff} = 0.547EI_{gross}$ for this cross section). The $EI_{elastic} = 0.9EI_{gross}$ contour is intended to show under what range of loads the use of gross section properties would be accurate or only modestly (roughly 10%) unconservative (i.e., predicting stiffer response with lower deformation). This range included axial loads up to $0.5P_{no}$ in pure compression but only up to $0.1M_{no}$ in pure bending, and covers primarily the higher axial load half of the allowable interaction diagram. Since the allowable cross section strength interaction diagram can roughly be considered to be the envelope of service load level loading, Fig. 7 indicates that EI_{gross} is likely too high for general use within an elastic analysis.

Similarly, the $EI_{elastic} = EI_{eff}$ contour indicates the range of loads where the use of EI_{eff} in an elastic analysis is accurate or conservative (i.e., predicting softer response with higher deformation). This range encompasses a larger range of loads than that for $EI_{elastic} = 0.9EI_{gross}$, including axial loads up to P_{no} in pure compression but only up to $0.2M_{no}$ in pure bending. Nonetheless, the range covers most of the envelope of service load level loading, particularly for axial compression greater than about $0.1P_{no}$. Thus, the results of Fig. 7 show that for this cross section, EI_{eff} is likely appropriate for columns with at least a modest amount of axial compression, but that a lower value is necessary for beams or columns with light gravity loads.

4. Behavior of members

Basing the flexural rigidity solely on cross-sectional behavior can lead to underestimates of the stiffness since it is common for the moment to vary across a member. For example, in a typical moment frame subjected to lateral load, the columns are subjected to double curvature bending with higher magnitude of bending moments at the member ends and lower magnitude of bending moments in the middle. Based on the observations from the previous section, the varying bending moment will result in varying stiffness. A stiffness representative of an average along the length is necessary to reasonably approximate the overall lateral drift deformations.

The generic beam-column shown in Fig. 8 will be used as the basis for analysis in this study. Member level analysis results, analogous the cross-section level results of Fig. 6, are shown in Fig. 9. In Fig. 9, the same SRC cross section as for Fig. 6 is used, but with the length of the column taken as 10 times the section depth (i.e., $L = 9.15$ m) and the stiffness of the rotational springs at the top and bottom of the column taken as infinite. The non-proportional loading is applied with an initial constant axial compression load of $P = 0.2P_{no} = 6900$ kN followed by the application of horizontal load up to $F_H = 2M_{no}/L = 964$ kN. The proportional loading is applied with a ratio of applied horizontal to vertical load of $F_H/P = 2M_{no}/(0.2P_{no}L) = 0.140$. The analyses are performed using the same constitutive relations as described above within a mixed beam finite element formulation [7]. Six elements were used along the length of the column, each with three integration points, a sufficiently dense finite element discretization to provide convergent results.

The observations for Fig. 9 are similar to those for Fig. 6. One difference is that the secant stiffness, $EI_{elastic}$, was determined iteratively such that the second-order elastic analysis provided the same peak deformation as the second-order inelastic analysis. An alternative approach is to select an elastic stiffness such that the elastic analysis provides the same peak moment as the inelastic analysis. In this simple case, where the peak moment and peak deformation occur at the same

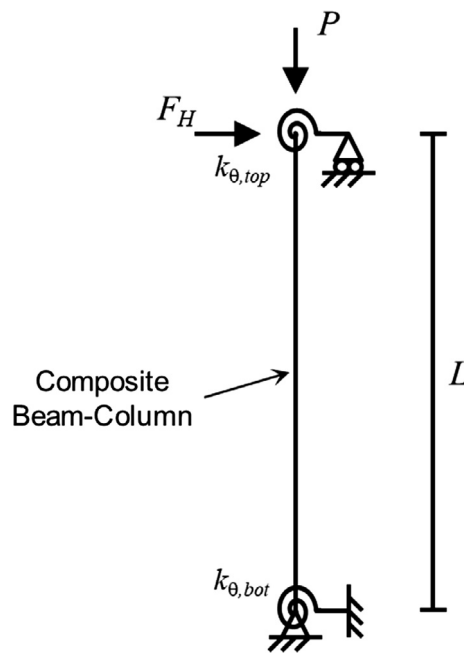


Fig. 8. Benchmark beam-column.

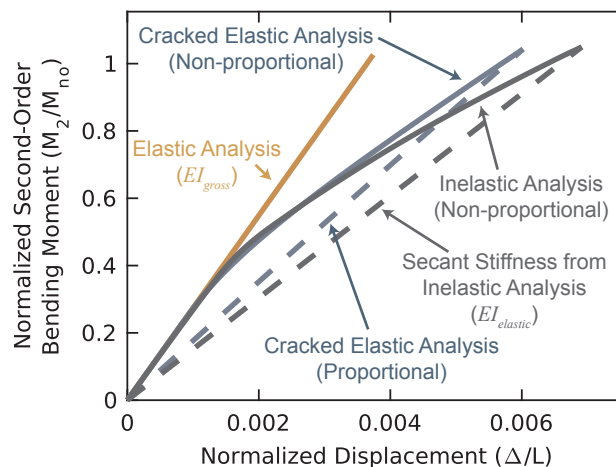


Fig. 9. Beam-column load-deformation analysis results.

location, the different approaches result in the same value.

The results of the computation of $EI_{elastic}$ for various pairs of axial compression and second-order bending moment is shown in Fig. 10, these results are presented in the same manner and are analogous to the cross-section level results of Fig. 7. The red dashed lines in Fig. 10 represent the nominal and allowable beam-column strength interaction diagrams. The allowable strength is being used again as a proxy for the upper bound of service level loading. Note that only three points are used for these diagrams in accordance with recommendations in the commentary to the AISC Specification [3]. In comparing Figs. 10 and 7, the fact that the contours from the beam-column results encompass a larger range of axial load and bending moment indicates that the cross-section level results underestimate the secant stiffness at the member level. Figures similar to Fig. 10 are presented for a wider range of composite cross sections in Denavit and Hajjar [7].

4.1. Influence of structural parameters

The preceding results have shown the influence of applied loads on the stiffness of composite columns, however, results have only been presented for one cross section. In this section, the influence of

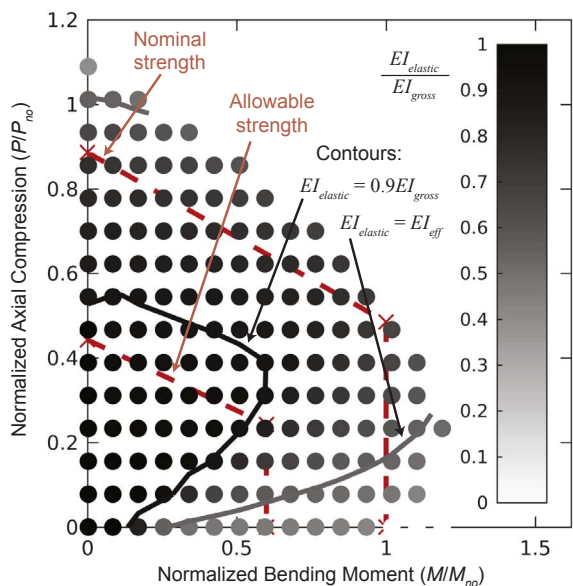


Fig. 10. Beam-column secant stiffness results.

structural parameters such as material and geometric properties will be investigated. The results in this section will use the same model and approach as the preceding results, but be based on columns of varying steel yield stress, concrete compressive strength, steel ratio, column length, and column boundary conditions. The base configuration, from which variations will be performed is a square CFT column with outside dimensions of 305 mm, steel ratio of $A_s/A_g = 0.10$, steel yield stress of $F_y = 350$ MPa, concrete compressive strength of $f'_c = 28$ MPa, column length of $L = 3.05$ m (10 times the section depth), and infinite spring rotational stiffness at top and bottom ($k_{\theta,top} = k_{\theta,bot} = \infty$), resulting in a top-to-bottom moment ratio of 1.0.

The results of the analyses are presented in Fig. 11 where each sub figure displays the results of several analyses where one parameter was varied from the base configuration. Note that variation in the moment ratio was obtained by varying the rotational stiffness of the bottom spring. For each analysis, $EI_{elastic}$ was determined at the specified axial compression load and a moment equal to $M_{no}/1.67$. This specific moment was chosen as being representative of the allowable moment for low axial load and what may roughly be deemed as the upper limit for service loading levels. This choice is appropriate for the development of recommendations of elastic flexural rigidity for determination of deflections at service loads, which is the focus of this paper. Other methods are appropriate for the development of recommendations for other purposes, for example, the elastic flexural rigidity for determination of internal forces for strength design [8]. It should be noted that concrete cracking is the primary inelastic effect at this level of load, as seen, for example, in the similarity of results between the cracked elastic analysis and inelastic analysis in Fig. 9. It is nonetheless important to conduct the inelastic analyses, as they better capture the continuum of behavior over a wide range of cases, including cases where the applied load does not cause cracking and those where other sources of inelasticity are significant.

The values of $EI_{elastic}$ were normalized using Eq. (18) (noting that for these analyses $E_s I_{sr} = 0$). The form of Eq. (18) was chosen since it is expected that the resulting design recommendations will be formulated as the summation of the gross properties of the steel components plus the product of a factor and the gross properties of the concrete component. The concrete is not the cause of all stiffness reductions since steel yielding can occur, but it is a convenient form for design and is consistent with existing design provisions.

$$C = \frac{EI_{elastic} - E_s I_{sr} - E_s I_{sr}}{E_c I_c} \quad (18)$$

In Fig. 11, the steel ratio was varied to as low as 0.01, which is the lower limit for composite columns in the AISC Specification [3]. This range includes cases that would not be considered compact. However, local buckling is neglected in this study, both by not modeling it in the inelastic analyses and by not including the strength reductions in strength calculations. The results were included in Fig. 11 because the steel ratio has a strong influence on the behavior of composite columns and there is value in some accounting of the full range. Specifically, it is expected that the recommendations developed in this study can be extended to noncompact and slender sections with minimal validation. Such a validation should consider the reduced likelihood of local buckling occurring at the lower level of loading investigated in this work. In fact, the validation could consider an even lower level of loading since the applied loads are based on strengths calculated neglecting the effect of local buckling in this study.

The normalization of applied loads and results in Fig. 11 allows for the comparison among the wide variety of cases investigated and allows for direct comparisons to the expected design recommendations, however, it does make identifying specific reasons for specific trends difficult. The identifiable trends are nonetheless important. First, in almost all cases the concrete contribution factor increases with increasing axial compression. Second, the cross-sectional properties (i.e., F_y , f'_c , and A_s/A_g) have a much larger influence on the results than the beam-column properties (i.e., column length and rotational spring stiffness). With the exception of the zero-length cases, which were run as a cross section, the length of the column had negligible effect on the resulting concrete contribution factor. Note, however, that all analyses in this study neglect shear deformations. Adjusting the stiffness of one of the rotational springs also had a negligible effect on the resulting concrete contribution factor. Only a slight increase is noted for moment ratios around 0.75 when a greater proportion of the length of the column has moments less than the maximum by a margin.

4.2. Parametric study

A wider parametric study is necessary to develop recommendations suitable for the range of material and geometric properties permitted in the design of composite columns. In the previous section, the influence of length and rotational spring stiffness was noted to be small. This observation was consistent with the results of analyses not presented here across a variety of different cross sections. Thus, all members evaluated in this parametric study will use a length-to-depth ratio of 10 and fixed-fixed boundary conditions ($k_{\theta,top} = k_{\theta,bot} = \infty$). The cross sections chosen for investigation in this work are categorized into four groups (1) CCFT, (2) RCFT, (3) SRC subjected to strong axis bending, and (4) SRC subjected to weak axis bending. Within these groups, material and geometric properties were selected to span practical ranges of steel strength, concrete strength, steel ratio, and reinforcing ratio for the SRC sections (CFTs with longitudinal reinforcing bars are excluded in this work). Parametric variations are given in Table 1 for the CFT cross sections and in Table 2 for the SRC cross sections.

Both the outside diameter of the CCFT cross sections and the outside dimension of the RCFT cross sections (only square sections were investigated) were taken as a constant 305 mm, noting that this choice is irrelevant once the results are normalized. The thickness was calculated to achieve specified steel ratio and did not necessarily conform to a commonly produced shape. Each parameter was run with each other parameter, resulting in (12 steel ratio values) \times (9 steel yield stress values) \times (14 concrete compressive strength values) = 1512 total analysis cases. Again, it is important to note that the range of steel ratios examined includes those associated with noncompact and slender sections despite the fact that local buckling is neglected in this study. Thus, the results of this study are only strictly applicable to compact

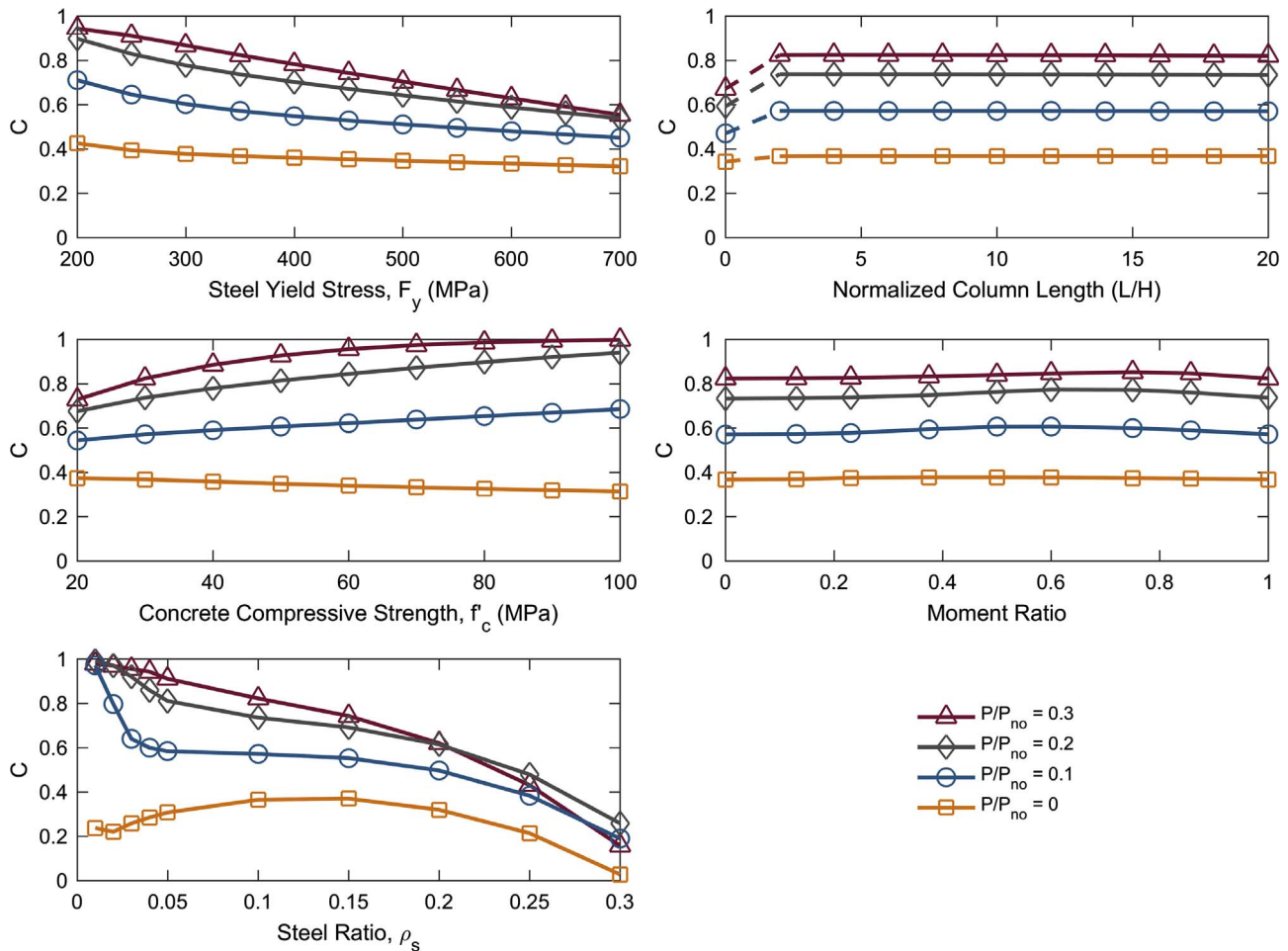


Fig. 11. Influence of structural parameters.

Table 1
Parametric variations for CFT members.

Parameter	Values
Steel ratio, A_s/A_g	0.01, 0.02, 0.03, 0.04, 0.05, 0.10, 0.15, 0.20, 0.25, 0.30, 0.35, and 0.40
Steel yield stress, F_y	240–520 MPa (increments of 35 MPa)
Concrete compressive strength, f'_c	20–111 MPa (increments of 7 MPa)

Table 2
Parametric variations for SRC members.

Parameter	Values
Steel shape	W360 × 1299, W360 × 990, W36 × 677, W360 × 314, W360 × 262, W360 × 196, W360 × 134, and W250 × 73 ($A_s/A_g = 0.198, 0.151, 0.103, 0.048, 0.040, 0.030, 0.020, \text{ and } 0.011$)
Steel yield stress, F_y	240–520 MPa (increments of 35 MPa)
Concrete compressive strength, f'_c	20–111 MPa (increments of 7 MPa)
Reinforcing configuration	4 #32, 12 #32, 20 #36, and 28 #36 ($A_s/A_g = 0.004, 0.012, 0.024, \text{ and } 0.034$)
Reinforcing yield stress, F_{ysr}	280 MPa, 420 MPa, and 520 MPa

sections or sections with stiffeners that prevent local buckling.

For the SRC cross sections, the outside dimensions were taken as 905 mm. A clear cover of 38 mm was provided from the outside face of the concrete to the ties. The longitudinal reinforcing steel was placed

symmetrically within the section and grouped in the corners with a clear spacing between the bars of 38 mm or 1.5 times the diameter of the bars, whichever was greater. The ties were spaced at 305 mm and are constructed with #10 bars when #32 longitudinal bars are used and #13 bars when #36 longitudinal bars are used. Each parameter was run with each other parameter, resulting in (8 steel shapes) × (9 steel yield stress values) × (14 concrete compressive strength values) × (4 reinforcing configurations) × (3 steel reinforcing yield stress values) = 12,096 total analysis cases.

For each case, an inelastic analysis was run subjecting the column first to constant axial compression, then to increasing horizontal force until the second-order bending moment reached $M_{no}/1.67$, at which point, the lateral drift at the top of the column was recorded. Then, the elastic stiffness, $EI_{elastic}$, corresponding to the lateral drift was determined as described above and normalized using Eq. (18). Results for the CCFT cross sections and SRC cross sections subjected to strong axis bending are shown in Fig. 12. The results for the other cross section types are similar and omitted for brevity. Each individual analysis is represented as one point. However, since the points overlap, histograms have been added for each unique steel ratio to clarify the distribution of the calculated concrete contribution factors.

Eqs. (19)–(22) were developed, by observation of the results shown in Fig. 12, as practical recommendations for the elastic flexural rigidity for use in determination of lateral deflections at service loads. These equations were developed considering that an underestimate of $EI_{elastic}$ is typically conservative, thus the minimum values of C in Fig. 12 were of greater importance than the maximum values. However, to prevent Eqs. (19)–(22) from being overly conservative, some cases do result in an overestimate of $EI_{elastic}$ when compared to the analytical results.

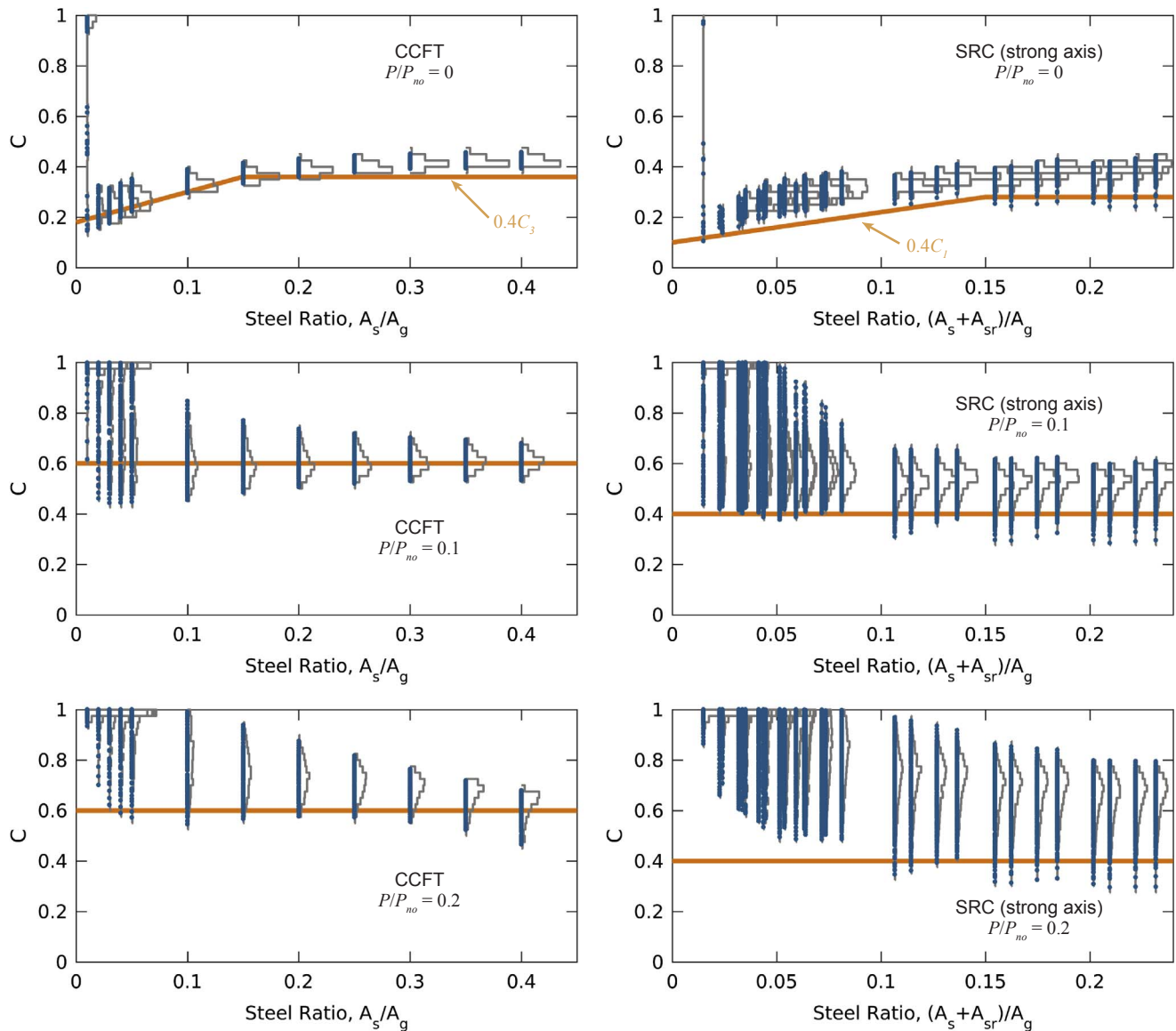


Fig. 12. Parametric study results – concrete contribution factor.

Also, as seen in previous results, the $EI_{elastic}$ generally increases with axial compression for service loading level. Thus, the results from the analysis with zero axial load were conservatively assigned a range of applicability of $P < 0.1P_{no}$ and the results from the analyses with $P = 0.1P_{no}$ or $0.2P_{no}$ were conservatively assigned a range of applicability of $P \geq 0.1P_{no}$.

In all cases, $EI_{elastic}$ is taken as the summation of the flexural rigidity for each of the components but the concrete component is factored down by some amount. That amount depends on the member type and level of axial compression. For the case of low axial compression, the factor is equal to 0.4 times the concrete contribution factor used in EI_{eff} , specifically, C_1 (Eq. (3b)) for SRC and C_3 (Eq. (4b)) for CFT. For the case of higher axial compression, the factor is a constant, specifically 0.4 for SRC and 0.6 for CFT. These factors are plotted in Fig. 12.

$$EI_{elastic} = E_s I_s + E_s I_{sr} + 0.4C_1 E_c I_c \quad (\text{SRC}, P < 0.1P_{no}) \quad (19)$$

$$EI_{elastic} = E_s I_s + E_s I_{sr} + 0.4E_c I_c \quad (\text{SRC}, P \geq 0.1P_{no}) \quad (20)$$

$$EI_{elastic} = E_s I_s + 0.4C_3 E_c I_c \quad (\text{CFT}, P < 0.1P_{no}) \quad (21)$$

$$EI_{elastic} = E_s I_s + 0.6E_c I_c \quad (\text{CFT}, P \geq 0.1P_{no}) \quad (22)$$

The results of Fig. 12 are useful for formulating design

recommendations, however, given that the goal of these recommendations is accurate determination of deflections, a comparison of the resulting deflections is a more direct assessment. The peak deformation at the target second-order moment from the inelastic analysis, $\Delta_{inelastic}$, is compared to the peak deformation at the same target moment from elastic analyses, $\Delta_{elastic}$, in Fig. 13. Two cases of elastic analyses were run, one using the $EI_{elastic}$ recommendations of Eqs. (19)–(22), and another using EI_{eff} as given in Eqs. (3) and (4).

For the CCFT results using $EI_{elastic}$, most results are grouped near $\Delta_{elastic}/\Delta_{inelastic} = 1$ indicating that the proposed recommendations are accurate. There is more dispersion in the SRC results, however, relatively few cases yield results where the elastic deformation is higher than that indicated by the inelastic analysis indicating that the proposed recommendations are conservative. The results using EI_{eff} show somewhat increased unconservative error. However, given the accuracy of determining the stiffness of structures, the use of EI_{eff} could potentially be justified. Such use could be efficient in the design processes since the elastic stiffness used to determine required strengths is also based on EI_{eff} [3].

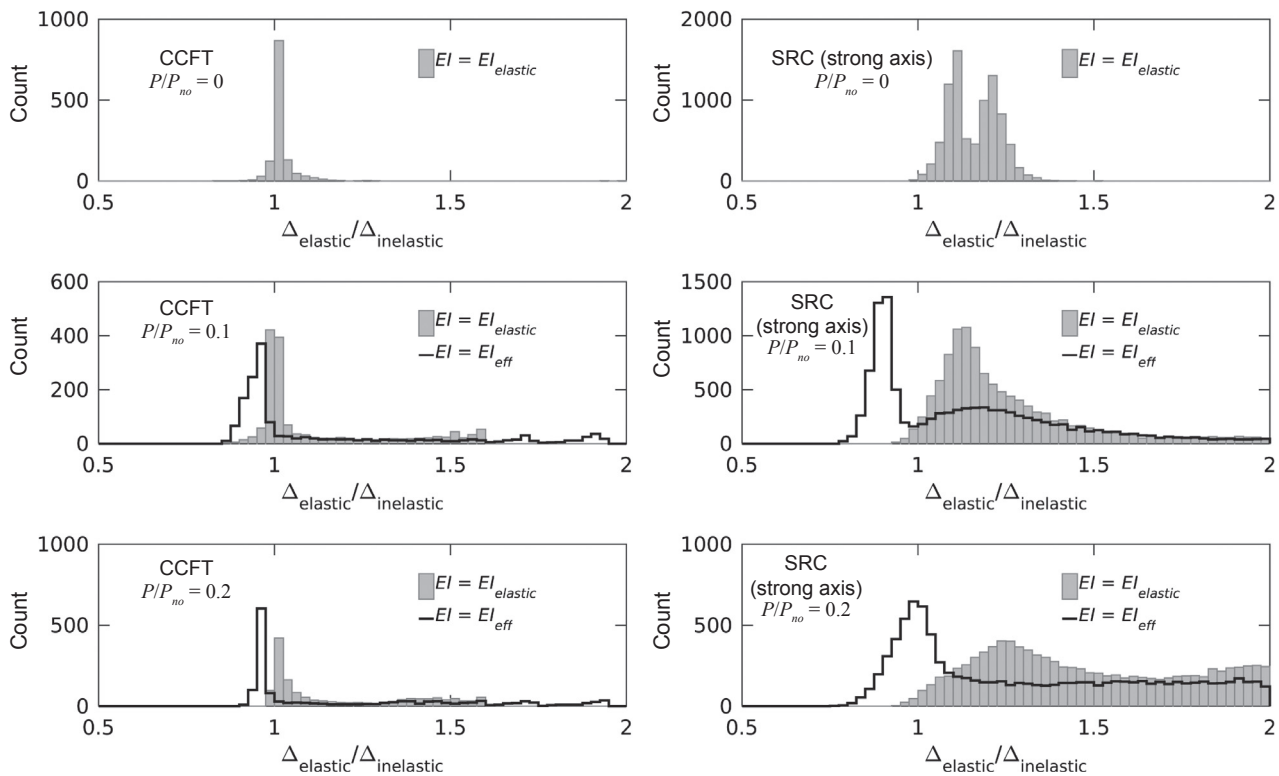


Fig. 13. Parametric study results – deformation.

5. Discussion

5.1. Behavior of frame systems

Just as aspects of member level behavior are missed by examining only cross section level behavior, aspects of frame level behavior are missed by examining only member level behavior. In an individual load case, different members within a frame will be loaded to different degrees. The more highly loaded members will experience more inelasticity while the more lightly loaded members will not. When examining system response such as story drifts, it is the average behavior that is important. Furthermore, the amount of axial compression within a column has a significant influence on the resulting stiffness. Axial compression has been held constant in the previous analyses (i.e., non-proportional loading), however, columns in frames may experience variation in axial load as lateral loads are applied. Unfortunately, the range of possible frame configurations makes a parametric study, such as was conducted at the member level, challenging.

5.2. Bounded solution

The focus of this paper has been to develop recommendations for creating elastic models of building structures that can accurately predict lateral drifts under service loads. In many cases of design, the level of approximation provided by the recommendations presented in this paper is suitable. However, for important or sensitive structures, it may be appropriate to conduct further analysis. There exists variation in the results (e.g., Fig. 13) which were used to calibrate the design recommendations. There also exists variation between the nominal and in-situ parameters. The elastic modulus of concrete, for instance, can be expected to have a coefficient of variation on the order of 12% [17]. Noting these variations, if additional analysis is deemed appropriate, a reasonable approach would be to identify expected upper and lower bounds of the flexural rigidity and use them to determine upper and lower bounds of deflections.

5.3. Elastic rigidities other than EI

This paper has also focused solely on the flexural rigidity, EI . However, other cross section rigidities contribute to the stiffness of the structure and their values should be carefully selected.

In the AISC *Specification* [3], the axial rigidity of composite columns, EA , is taken as the summation of the elastic axial rigidities of each component (Eq. (23)). This is in agreement with most studies as summarized by Schiller et al. [22].

$$EA_{\text{elastic}} = E_s A_s + E_s A_{sr} + E_c A_c \quad (23)$$

The shear rigidity, GA , is necessary when shear deformations are included in the elastic model (i.e. Timoshenko beam theory). Tomii and Sakino [25] performed experiments on RCFT members and recommended an expression for GA . For CCFT and SRC members, no suitable expressions for GA have been found in the literature, so it is recommended to use the shear rigidity of either the steel or concrete section alone.

The torsional rigidity, GJ , is necessary for three-dimensional analyses. For CFT members, Perea [19] developed expressions for the torsional rigidity based on a series of full scale slender beam-column tests. For SRC members, no suitable expressions for GJ have been found in the literature, so it is recommended to use the torsional rigidity of either the steel or concrete section alone.

6. Conclusions

This paper presents the results of a detailed study of the stiffness of composite columns at the cross section and member levels with the goal of developing recommendations for elastic design procedures. The secant stiffness was seen to vary with both the type of loading (which influences the location of the neutral axis) and the magnitude of loading. Thus, the choice of elastic flexural rigidity depends on the purpose of the elastic analysis and the type of behavior that is expected to be captured. Specific practical design recommendations were developed for the elastic flexural rigidity for determination of deflections

at service loads (Eqs. (19)–(22)). The ability to estimate lateral drifts at service loads is important for building design and existing recommendations are lacking. The form of the recommended expressions for the elastic flexural rigidity was taken as the gross flexural rigidity of the steel and reinforcement plus a factor times the gross flexural rigidity of the concrete. The factor applied to the concrete contribution was taken as the main variable in the development of the recommendations. This factor was shown to vary significantly with cross section properties such as steel ratio and concrete compressive strength, and less so for beam-column properties such as length and boundary conditions. Nonetheless, a broad parametric study showed that the simple recommended expressions were suitable for capturing the behavior in a conservative manner, however, further experimental validation is still warranted.

Acknowledgments

This material is based upon work supported by the National Science Foundation under Grant Nos. CMMI-0530756 and CMMI-0619047 as part of the George E. Brown, Jr. Network for Earthquake Engineering Simulation (NEES), the American Institute of Steel Construction, the Georgia Institute of Technology, the University of Illinois at Urbana-Champaign, and Northeastern University.

References

- [1] Abdel-Rahman N, Sivakumaran KS. Material properties models for analysis of cold-formed steel members. *J Struct Eng ASCE* 1997;123(9):1135–43.
- [2] ACI. Building code requirements for structural concrete and commentary. Farmington Hills (MI): American Concrete Institute; 2014.
- [3] AISC. Specification for structural steel buildings. Chicago (Illinois): American Institute of Steel Construction; 2016.
- [4] Avşar Ö, Bayhan B, Yakut A. Effective flexural rigidities for ordinary reinforced concrete columns and beams. *Struct Des Tall Spec Build* 2014;23(6):463–82.
- [5] CEN. Eurocode 4: design of composite steel and concrete structures – Part 1–1: General rules and rules for buildings. Brussels (Belgium): European Committee for Standardization; 2004.
- [6] Chang GA, Mander JB. Seismic energy based fatigue damage analysis of bridge columns: Part I – Evaluation of seismic capacity. Buffalo (New York): National Center for Earthquake Engineering Research, Department of Civil Engineering, State University of New York at Buffalo; 1994.
- [7] Denavit MD, Hajjar JF. Characterization of behavior of steel-concrete composite members and frames with applications for design. Newmark structural laboratory report series, Newmark structural laboratory report NSEL-034. Urbana (Illinois) University of Illinois at Urbana-Champaign; 2014.
- [8] Denavit MD, Hajjar JF, Perea T, Leon RT. Stability analysis and design of composite structures. *J Struct Eng ASCE* 2016;142(3):04015157.
- [9] Elwood KJ, Eberhard MO. Effective stiffness of reinforced concrete columns. *ACI Struct J* 2009;106(4):476–84.
- [10] Galambos TV, Ketter RL. Columns under combined bending and thrust. *J Eng Mech Div ASCE* 1959;85(2):1–30.
- [11] Khuntia M, Ghosh SK. Flexural stiffness of reinforced concrete columns and beams: analytical approach. *ACI Struct J* 2004;101(3):351–63.
- [12] Khuntia M, Ghosh SK. Flexural stiffness of reinforced concrete columns and beams: experimental verification. *ACI Struct J* 2004;101(3):364–74.
- [13] Kumar R, Singh Y. Stiffness of reinforced concrete frame members for seismic analysis. *ACI Struct J* 2010;107(05):607–15.
- [14] Leon RT, Kim DK, Hajjar JF. Limit state response of composite columns and beam-columns Part 1: Formulation of design provisions for the 2005 AISC specification. *Eng J AISC* 2007;44(4):341–58.
- [15] MacGregor JG, Hage SE. Stability analysis and design of concrete frames. *J Struct Div ASCE* 1977;103(10):1953–70.
- [16] Mirza SA. Flexural stiffness of rectangular reinforced concrete columns. *ACI Struct J* 1990;87(4):425–35.
- [17] Mirza SA, Skrabek BW. Statistical analysis of slender composite beam-column strength. *J Struct Eng ASCE* 1992;118(5):1312–32.
- [18] Park R, Paulay T. Reinforced concrete structures. John Wiley & Sons Inc.; 1975.
- [19] Perea T. Analytical and experimental study on slender concrete-filled steel tube columns and beam-columns. Ph.D. Dissertation. Atlanta (Georgia): School of Civil and Environmental Engineering, Georgia Institute of Technology; 2010.
- [20] Perea T, Garcia MA, Ruiz-Sandoval ME, Leon RT, Denavit MD, Hajjar JF. Calibration of the elastic flexural rigidity from ambient vibration measurements for a building with encased composite columns. In: Proceedings of the 8th international conference on composite construction in steel and concrete, Jackson, Wyoming; 2017.
- [21] Roeder CW, Lehman DE, Bishop E. Strength and stiffness of circular concrete-filled tubes. *J Struct Eng ASCE* 2010;136(12):1545–53.
- [22] Schiller PH, Hajjar JF, Gourley BC. Expressions for the elastic rigidity of rectangular concrete-filled steel tube beam-columns. Structural engineering report no. ST-94-2. Minneapolis (Minnesota) Department of Civil Engineering, University of Minnesota; 1994.
- [23] Tikka TK, Mirza SA. Nonlinear equation for flexural stiffness of slender composite columns in major axis bending. *J Struct Eng ASCE* 2006;132(3):387–99.
- [24] Tikka TK, Mirza SA. Nonlinear EI equation for slender composite columns bending about the minor axis. *J Struct Eng ASCE* 2006;132(10):1590–602.
- [25] Tomii M, Sakino K. Experimental studies on concrete filled square steel tubular beam-columns subjected to monotonic shearing force and constant axial force. *Trans Archit Inst Jpn* 1979;281:81–90.
- [26] Tort C, Hajjar JF. Reliability-based performance-based design of rectangular concrete-filled steel tube (RCFT) members and frames. Structural engineering report no. ST-07-1. Minneapolis (Minnesota) Department of Civil Engineering, University of Minnesota; 2007.